AGU PUBLICATIONS

JGR

Journal of Geophysical Research: Atmospheres

RESEARCH ARTICLE

10.1002/2013JD021258

Key Points:
- Climate system does not respond symmetrically to forcing increase and decrease
- Oceanic circulation and feedbacks affected differently by solar forcing changes
- Informs how to set up geoengineering simulations from single-forcing simulations

Correspondence to:
N. Schaller,
nathalie.schaller@ouce.ox.ac.uk

Citation:
Schaller, N., J. Sedláček, and R. Knutti (2014), The asymmetry of the climate system's response to solar forcing changes and its implications for geoengineering scenarios, *J. Geophys. Res. Atmos.*, *119*, doi:10.1002/2013JD021258.

Received 26 NOV 2013
Accepted 8 APR 2014
Accepted article online 10 APR 2014

The asymmetry of the climate system's response to solar forcing changes and its implications for geoengineering scenarios

N. Schaller[1,2], J. Sedláček[1], and R. Knutti[1]

[1]Institute for Atmospheric and Climate Science, ETH, Zurich, Switzerland, [2]Environmental Change Institute, Oxford University Centre for the Environment, Oxford, UK

Abstract Motivated by proposals to compensate CO_2-induced warming with a decrease in solar radiation, this study investigates how single-forcing simulations should be combined to best represent the spatial patterns of surface temperature and precipitation of idealized geoengineering scenarios. Using instantaneous and transient simulations with changing CO_2 and solar forcings, we show that a geoengineering scenario, i.e., a scenario where the solar constant is reduced as CO_2 concentrations are increased, is better represented by subtracting the response pattern of a solar forcing increase simulation from the response pattern of a CO_2 forcing increase simulation, than by adding the response pattern of a solar forcing decrease simulation to a CO_2 forcing increase simulation. The reason is a asymmetric response of the climate system to a forcing increase or decrease between both hemispheres. In particular, the Atlantic meridional overturning circulation responds faster to a solar forcing decrease compared to a solar forcing increase. Further, the climate feedbacks are state and region dependent, which is particularly apparent in the polar regions due to the sea ice-albedo feedback. The importance of understanding the local response of the climate system to geoengineering and single-forcing scenarios is highlighted, since these aspects are hardly discernible when only global mean values are considered.

1. Introduction

Geoengineering has been proposed as a way to counteract the temperature increase caused by increases in CO_2 concentrations with the injection of aerosol precursors like sulphur dioxide in the stratosphere, or more simply, by a decrease in the solar constant [*Schneider*, 1996; *Crutzen*, 2006; *Vaughan and Lenton*, 2011]. Whether geoengineering techniques should be applied to prevent unwanted global warming remains a highly debated question and is not the topic of this study. Nevertheless, geoengineering proposals bring interesting questions to the climate modeling world. For example, even if global mean temperature anomalies are close to zero in geoengineering scenarios [*Wigley*, 2006], the spatial response of many climate variables, including surface temperature and precipitation, can be substantial on a regional scale [*Bala et al.*, 2008; *Ricke et al.*, 2010; *Schmidt et al.*, 2012; *Kravitz et al.*, 2013a; *Tilmes et al.*, 2013]. Thereby, more or less realistic geoengineering scenarios have been developed and studied. For example, *Ban-Weiss and Caldeira* [2010] focused on optimizing the latitudinal distribution of sulphate aerosols in the stratosphere that would most closely achieve a low-CO_2 climate, while *MacMartin et al.* [2013] investigated how optimizing the latitudinal and seasonal distribution of solar reduction can improve the fidelity with which solar radiation management counteracts CO_2-induced climate change, assuming a linearity in the response to forcings. Recently, results have been published from the Geoengineering Model Intercomparison Project (GeoMIP) project [*Kravitz et al.*, 2011], which considers idealized geoengineering simulations, i.e., where solar radiation management is simply achieved by reducing the solar constant in the climate model simulation. For the first time, robust responses across Earth System Models (ESMs) to such idealized geoengineering simulations have been described [*Schmidt et al.*, 2012; *Kravitz et al.*, 2013a; *Tilmes et al.*, 2013]. A particular attention has been given to changes in the hydrological cycle [*Tilmes et al.*, 2013; *Kravitz et al.*, 2013b]. Consistent across ESMs, *Tilmes et al.* [2013] identified a reduction in global precipitation by around 4.5% and significant reductions over monsoonal land regions, even when global mean temperature change is zero. Besides changes in net radiation which control evaporative processes at the surface, the reduction of evapotranspiration over land is primarily caused by reduced transpiration through the leaves of plants with increasing CO_2 concentrations changes [*Tilmes et al.*, 2013; *Fyfe et al.*, 2013].

Bala et al. [2008] not only investigated the climate response to such idealized geoengineering simulations but they also contrasted the responses of the climate system to increases in CO_2 and solar forcings individually. Investigating idealized single-forcing simulations is helpful to understand basic physical mechanisms in the climate system, and recently, a number of studies have focused on quantifying the response of the hydrological cycle, in particular, to CO_2 and solar forcings [*Bala et al.*, 2010; *Andrews et al.*, 2010; *Cao et al.*, 2012]. In the field of detection and attribution of climate change, single-forcing simulations are commonly performed along with simulations including all observed forcing agents [e.g., *Stott et al.*, 2000; *Meehl et al.*, 2004; *Barnett et al.*, 2005]. A simulation with only one forcing agent is not only helpful to understand the climate response to this forcing agent, as stated above, it also allows the attribution of observed climate change to the different forcing agents [*Stott et al.*, 2006]. In this case, single-forcing simulations are simply added together. The assumption that the response to different forcings adds linearly works well since the forcings applied are relatively weak [*Meehl et al.*, 2004]. However, the assumption of linear additivity might not always be valid as different forcing agents can interact with each other in all-forcings simulations, and these processes are not simulated when single-forcing simulations are added together. For the early twentieth century, *Meehl et al.* [2003] showed that the sea surface temperature response of their model to solar forcing is amplified when it is combined with anthropogenic forcings. Since solar forcing acts in areas where sunlight reaches the surface (i.e., solar forcing is spatially heterogeneous), this leads to regional feedbacks because of local differences in temperature gradients, circulation regimes, and cloud cover. In the presence of increased CO_2, which is spatially homogeneous, those regional feedbacks are amplified [*Meehl et al.*, 2003]. Pattern-scaling techniques as well make the assumption that the responses to different forcing agents or to forcing agents of different intensity add linearly [*Mitchell*, 2003]. New studies, however, identified significant nonlinearities in the response of temperature and precipitation to CO_2 forcing, both on a global and regional scale [*Good et al.*, 2011; *Jonko et al.*, 2012; *Schaller et al.*, 2013; *Chadwick and Good*, 2013].

In this study, similarly as in *Bala et al.* [2008], we perform model simulations with geoengineering and single-forcing scenarios. It is currently not clear, given the available literature, whether it would be defensible to combine CO_2-only and solar forcing-only simulations in order to obtain the response to a geoengineering scenario. Due to limited CPU time or storage availability, it might be tempting to perform only single-forcing simulations and use them for several purposes, e.g., to investigate on the one hand the individual effects of CO_2 and solar forcings on precipitation and on the other hand to investigate the climate response to a geoengineering simulation. Our goal is therefore to test whether the responses to single-forcing simulations can be combined to represent the response to a geoengineering scenario. In particular, we will test whether the single-forcing simulation for the solar case should be performed with a solar forcing increase, which has the advantage to compare the climate response of the system to CO_2 concentration increase, or with a solar forcing decrease, as is actually occurring in geoengineering simulations, for example, in the GeoMIP project [*Kravitz et al.*, 2013a]. Thereby, the implicit question is whether the climate system responds symmetrically to a forcing increase or decrease. Because the assumption of linearity is often made, one would expect that reversing the sign of the forcing would simply reverse the sign of the response. Testing the symmetry of the climate system response to cooling and warming scenarios will also shed light on the limits of pattern scaling and attribution techniques. Finally, as in the GeoMIP project, we will also quantify the differences for both instantaneous and transiently evolving forcings [*Kravitz et al.*, 2011].

2. Climate Model Simulations

Idealized instantaneous and transient simulations are performed with the National Center for Atmospheric Research Community Climate System Model version 3.5 (CCSM3.5), which is a global coupled atmosphere-ocean general circulation model (AOGCM) [*Collins et al.*, 2006; *Gent et al.*, 2010]. The spatial resolution in the atmosphere is 1.9° in latitude and 2.5° in longitude, with 26 levels in the vertical. The resolution in the ocean is nominally 1° with 60 vertical levels. CCSM3.5 is an interim version before the release of CCSM4 [*Gent et al.*, 2011], and the main improvement from CCSM3 [*Collins et al.*, 2006] is that the atmosphere component switched from a spectral to a finite volume dynamical core [*Gent et al.*, 2010]. CCSM4, which is the most similar version of CCSM3.5, has been evaluated, and *Gent et al.* [2011] summarized that in the atmosphere component, the tropical precipitation frequency distribution and the El Niño–Southern Oscillation were improved, although the El Niño–Southern Oscillation amplitude is still too large compared to observations. CCSM4 has global mean temperature bias of 0.48°C for the

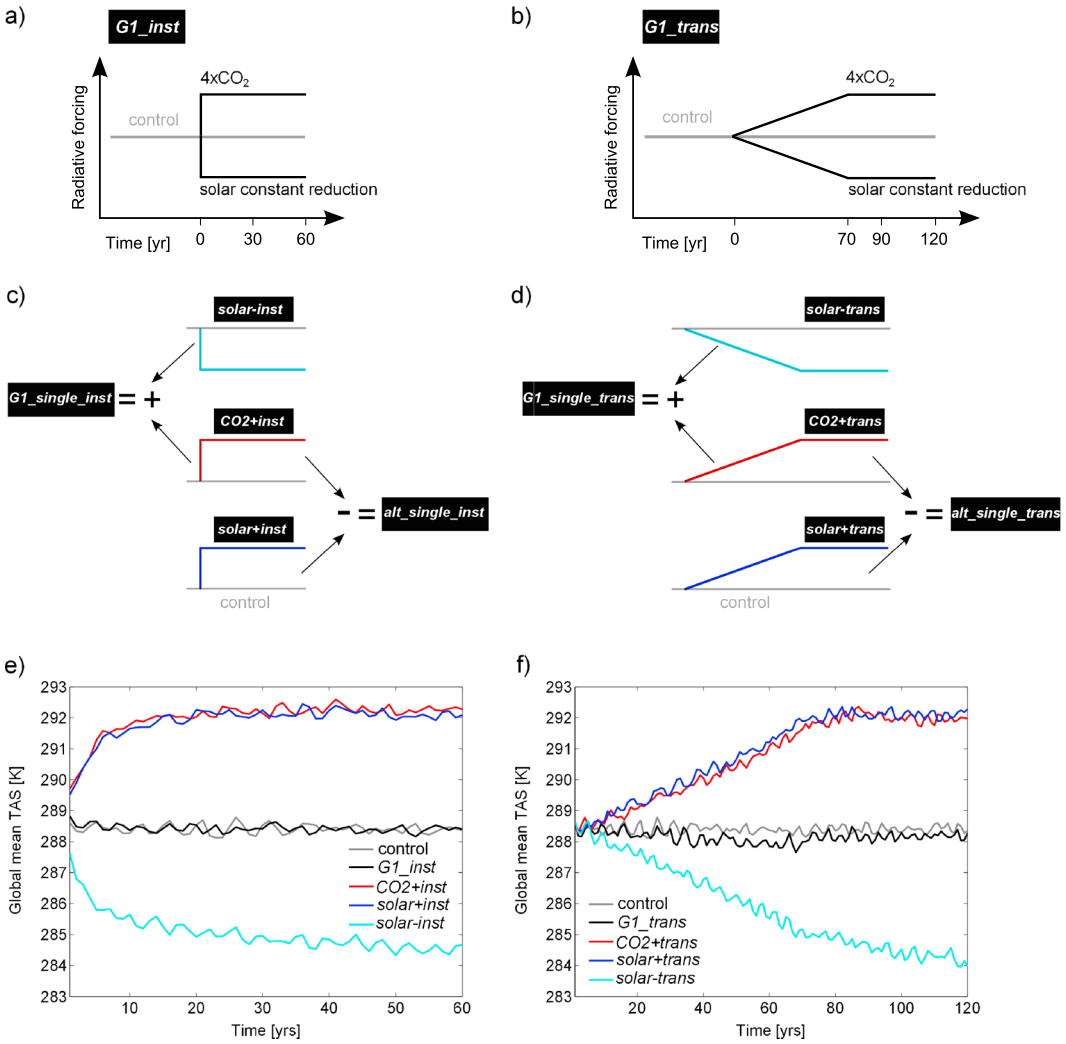

Figure 1. Overview of the simulations used in the study. (a and b) Schematic illustration on how the geoengineering simulation are setup in the instantaneous and transient case, respectively. (c and d) The single-forcing simulations and how they are combined to reconstruct a geoengineering response pattern. Thereby, the same axes as in Figures 1a and 1b, respectively, apply. (e and f) Global annual mean surface air temperature in the performed simulations and the control run.

period 1850–2005 [*Gent et al.*, 2011]. The global mean surface air temperature drift is about 0.01°C/100 yr [*Sedlacek et al.*, 2012]. CCSM3.5 includes a different overflow parameterization as in CCSM4, and therefore, the North Atlantic deep water circulation reaches to the bottom of the ocean between 15°N and 55°N; the mean transport through Drake Passage is too large, and the deep Meridional Overturning Circulation (MOC) in the Southern Hemisphere is probably too deep compared to observations [*Gent et al.*, 2011]. CCSM4, and therefore CCSM3.5 as they share the same sea ice component, matches well the observed September Arctic sea ice extent from 1979 to 2005, although sea ice area extends too far south in the North Atlantic and in the North Pacific Ocean, as well as too far north around Antarctica [*Gent et al.*, 2011]. *Sedlacek et al.* [2012] showed that sea ice thickness and extent in CCSM4 agrees well with observations.

In addition to a 600 year steady state present-day (i.e., 1990, CO_2 concentration of 355 ppmv) control simulation, eight different simulations are performed. First, a 60 year simulation is run, where initial CO_2 concentrations are instantaneously quadrupled and the solar constant is instantaneously reduced by 61.4 W/m^2 (the adjusted radiative forcing is lower due to the geometry and albedo of the Earth), such that the anomaly in global annual mean surface temperature averaged over the last 30 years is close to zero (−0.01 K). This reference geoengineering simulation will be referred to as "*G1_inst*" in the rest of the study (see Figure 1a) and has the same setup as the G1 scenario in GeoMIP [*Kravitz et al.*, 2011]. Second, a simulation with the

Table 1. Description of the Forcing Applied in the Individual Simulations Along With Global Annual Mean Anomalies for Surface Air Temperature (TAS (K)) and Net TOA Energy Flux (TOA Net (W/m^2)), Averaged Over the Last 30 Years of Each Simulations[a]

	Forcing Applied	TAS	TOA Net
G1_inst	abrupt 4×CO_2 and 61.4 W/m^2 increase in solar constant	−0.01	0.03
G1_trans	transient 4×CO_2 and 61.4 W/m^2 increase in solar constant	−0.24	0.19
CO2+inst	abrupt 4×CO_2	3.85	2.3
CO2+trans	transient 4×CO_2	3.56	2.03
solar+inst	abrupt 61.4 W/m^2 increase in solar constant	3.71	2.18
solar+trans	transient 61.4 W/m^2 increase in solar constant	3.7	2.08
solar-inst	abrupt 61.4 W/m^2 decrease in solar constant	−3.74	−2.12
solar-trans	transient 61.4 W/m^2 decrease in solar constant	−4.07	−1.91

[a]Energy fluxes are defined as positive downward.

same forcing changes as *G1_inst* is performed, with the difference that CO_2 concentrations increase and the solar constant decreases transiently. CO_2 concentration increases by a rate of 2% per year and the quadrupling of CO_2 is reached during year 70. The solar constant decreases transiently to reach a negative change of 61.4 W/m^2 at the surface, also in year 70. This simulation will be referred to as "*G1_trans*" (see Figure 1b) and is similar to the G2 scenario in GeoMIP, apart from the fact that in G2, the rates of CO_2 and solar forcing changes are lower by a factor of 2 [*Kravitz et al.*, 2011].

Then, to identify the most appropriate way to combine individual CO_2 and solar forcing simulations to best represent a geoengineering scenario, six single-forcing simulations are performed. Of the two CO_2 forcing simulations, one is an instantaneous quadrupling of CO_2 ("*CO2+inst*") and the other one has a 2% per year CO_2 concentration increase, and quadrupling of CO_2 is reached after 70 years ("*CO2+trans*"), as in *G1_inst* and *G1_trans*, respectively. Similarly, a simulation with instantaneous solar constant increase of 61.4 W/m^2 (labeled "*solar+inst*") and a transient solar constant increase simulation (labeled "*solar+trans*") are performed. In addition, the same solar forcing simulations are executed but with instantaneous and transient solar constant decreases (labeled "*solar-inst*" and "*solar-trans*"). The instantaneous and transient simulations are 60 and 120 years long, respectively, and the transient simulations have constant forcing after year 70. A summary of these simulations is presented in Table 1 and illustrated in Figure 1.

The first possibility to combine the single-forcing simulations is to add the 30 years mean fields of the solar forcing decrease simulations, *solar-inst* and *solar-trans*, respectively, to the 30 years mean fields of the *CO2+inst* and *CO2+trans* simulations. This is equivalent, in terms of forcing applied, to *G1_inst* and *G1_trans* and will be labeled "*G1_single_inst*" and "*G1_single_trans*", respectively. An alternative way to combine single-forcing simulations is to subtract the 30 years mean fields of the solar forcing increase simulations, *solar+inst* and *solar+trans*, respectively, from the 30 years mean fields of the *CO2+inst* and *CO2+trans* simulations. These alternative combinations of single-forcing simulations will be referred to as "*alt_single_inst*" and "*alt_single_trans*", respectively. A sketch of the single-forcing simulations and their combinations is presented in Figures 1c and 1d. Time series of the global annual mean surface temperature in the simulations are shown in Figures 1e and 1f.

The values for each variable shown in this study are anomalies (defined as the difference with a 30 year average in the control simulation) averaged over years 31–60 for the instantaneous simulations and over years 91–120 for the transient simulations. All fluxes are defined as positive downward.

3. Results and Discussions

The simulations performed for this study allow us to investigate three different aspects of the response of the climate system to forcing agents: (i) CO_2 forcing versus solar forcing, (ii) warming versus cooling of the surface, and (iii) transient versus near-equilibrium response. In this study, the focus is given to the second and third aspects. Some aspects of the effects of CO_2 forcing versus solar forcing are presented by *Schaller et al.* [2013]. They found that the response to individual forcings cannot simply be added linearly to estimate the responses to the combined forcing and described the different physical processes occurring as a response to a surface warming caused by CO_2 or solar forcing increases of the same magnitude.

Table 2. Global Annual Mean Anomalies for Different Variables Averaged Over the Last 30 Years of Each Geoengineering and Combined Geoengineering Simulations[a]

	G1_inst	*G1_single_inst*	*alt_single_inst*	*G1_trans*	*G1_single_trans*	*alt_single_trans*
TOA SW net (W/m^2)	−8.18	−8.2	−8.22	−8.37	−9.46	−9.08
TOA LW net (W/m^2)	8.22	8.38	8.34	8.56	9.58	9.03
TOA net (W/m^2)	0.03	0.18	0.12	0.19	0.12	−0.05
Surf SW net (W/m^2)	−4.18	−4.51	−4.16	−4.27	−5.63	−5.02
Surf LW net (W/m^2)	0.69	1.2	0.65	0.63	1.48	1.02
Sensible heat (W/m^2)	−0.32	−0.56	−0.23	−0.41	0.42	0.83
Latent heat (W/m^2)	3.84	4	3.81	4.22	3.87	3.09
Surface net (W/m^2)	0.02	0.14	0.07	0.18	0.13	−0.08
Precip (mm/day)	−0.13	−0.14	−0.13	−0.15	−0.13	−0.11
TAS (K)	−0.01	0.11	0.14	−0.24	−0.51	−0.14

[a]Energy fluxes are defined as positive downward.

3.1. Warming Versus Cooling

As a first step, we consider the responses to instantaneous and transient forcing changes separately and assess for both cases the most appropriate way to combine the CO_2 and solar forcing simulations to best represent *G1_inst* and *G1_trans*. Thereby, we choose to assess which combination is more appropriate by considering the global annual mean anomalies in a set of variables and the anomaly patterns of surface air temperature and total precipitation. Other metrics could be chosen of course. It is important to stress that *G1_single_inst*, *G1_single_trans*, *alt_single_inst*, and *alt_single_trans* are not simulations and are obtained mathematically. Anomalies for all possible variables could theoretically be calculated, but they cannot be interpreted like the other actual geoengineering simulations as they do not necessarily represent any physical states. Their sole purpose is therefore to identify which combination is the most appropriate to represent *G1_inst* and *G1_trans* based on the criteria described above. Physical mechanisms that explain the results will therefore be inferred only from the actual simulations, *G1_inst*, *G1_single_inst*, *CO2+inst*, *CO2+trans*, *solar+inst*, *solar+trans*, *solar-inst*, and *solar-trans*.

Overall, the global annual mean values presented in Table 2 are close in *G1_inst*, *G1_single_inst*, and *alt_single_inst* and in *G1_trans*, *G1_single_trans*, and *alt_single_trans*, although the geoengineering simulations, i.e., *G1_inst* and *G1_trans*, are, in general, colder than the combined ones. This is similar to the result described by *Meehl et al.* [2003] that the response to solar forcing is amplified when combined with a CO_2 forcing as mentioned in section 1. The *alt_single_trans* would be the exception, which is due to the fact that the simulation has not yet reached equilibrium, as will be discussed further in the following section. Maps of temperature and precipitation anomalies for all geoengineering simulations are presented in Figures 2 and 3. Consistent with previous studies, although global annual mean surface temperature is stabilized, there is a clear positive temperature anomaly in both polar regions while the lower latitudes experience a cooling in *G1_inst* and *G1_trans* [see, for instance, *McCusker et al.*, 2012]. A similar pattern is found for the net top of atmosphere (TOA) flux (not shown), indicating that solar forcing dominates the response in low latitudes while CO_2 forcing dominates in high latitudes, as expected [*Schmidt et al.*, 2012; *Kravitz et al.*, 2013a]. CO_2 forcing traps heat in the system at all latitudes and during day and night, whereas a decrease in solar forcing acts only during the day, all year round at the equator but only during the summer season at high latitude [*Govindasamy and Caldeira*, 2000]. Further, in *G1_inst* and *G1_trans*, the state of the climate system does not change much, except for some adjustments between land and ocean as well as between low and high latitudes, due to the different "areas of action" of both forcing agents. Most importantly, as global mean surface temperature remains constant in these simulations, this implies that feedback processes will be largely inactive. Generally, the patterns of precipitation anomalies show significant negative residuals over the oceans and some inhabited areas. Similarly as in *Tilmes et al.* [2013], CCSM3.5 has significant negative precipitation anomalies over South America, Europe, parts of North America, and Southeast Asia. The positive precipitation anomalies are generally not significant, as in *Tilmes et al.* [2013]. *Tilmes et al.* [2013] and *Fyfe et al.* [2013], for example, highlighted the changes in evapotranspiration as a major process to explain the dry anomalies in geoengineering simulations. In solar forcing simulations, due to increasing incoming shortwave radiation, latent heat flux increases. Latent heat flux also increases in CO_2 forcing simulations but less so as rising CO_2 concentrations cause plants to close their stomata and hence reduces evapotranspiration and precipitation over land [*Tilmes et al.*, 2013]. Stomatal resistance is parameterized in CCSM3.5 [*Lawrence et al.*, 2007].

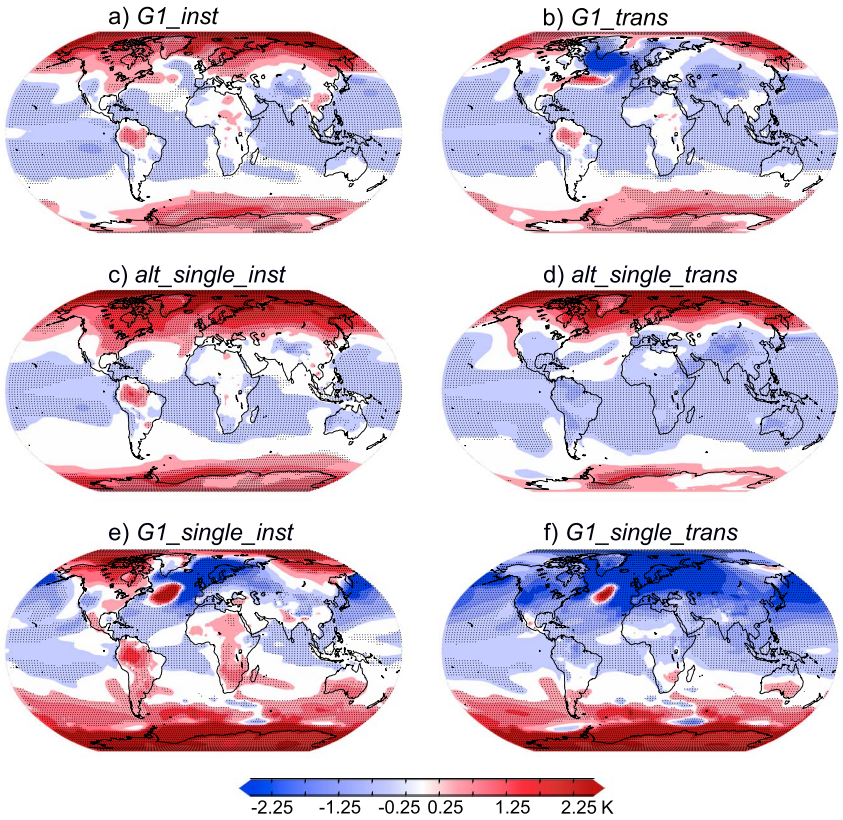

Figure 2. Maps of annual mean surface temperature anomaly (K) averaged over the last 30 years of the respective geoengineering and combined geoengineering simulations: (a) *G1_inst*, (b) *G1_trans*, (c) *alt_single_inst*, (d) *alt_single_trans*, (e) *G1_single_inst*, and (f) *G1_single_trans*. Stippling indicates regions where the changes are significant at the 1% level. Significance level is estimated by using a Student's *t* test.

Fischer et al. [2011] showed that the transpiration is actually reduced due to changes in stomatal conductance resulting from enhanced CO_2 concentrations, but this effect is compensated by enhanced bare soil evaporation in this model version. Therefore, the negative precipitation anomalies in *G1_inst*, *G1_trans*, and all four combined simulations are likely to be underestimated.

The location and amplitude of the anomalies of *G1_inst* and *G1_trans* are more similar to those of *alt_single_inst* and *alt_single_trans*, respectively, than to those of *G1_single_inst* and *G1_single_trans*. The area weighted root-mean-square error (RMSE) for significant differences from the control run between the response pattern of *G1_inst* and *alt_single_inst* for surface temperature as shown in Figure 2 is 0.47, while RMSE = 1.17 between *G1_inst* and *G1_single_inst*. The differences are smaller for precipitation, with RMSE = 0.28 between *G1_inst* and *alt_single_inst* and RMSE = 0.47 between *G1_inst* and *G1_single_inst*.

The same is true for the transient simulations: for surface temperature, RMSE = 0.82 between *G1_trans* and *alt_single_trans*, and RMSE = 1.42 between *G1_trans* and *G1_single_trans*. Again, the response patterns for precipitation between the combined simulations and the geoengineering simulation are more similar: RMSE = 0.32 between *G1_trans* and *alt_single_trans*, and RMSE = 0.48 between *G1_trans* and *G1_single_trans*. Overall, the regional anomalies in *G1_single_inst* and *G1_single_trans* are overestimated compared to *G1_inst* and *G1_trans* and to some extent show different temperature and precipitation patterns.

The main reason why geoengineering simulations are better represented by *alt_single_inst* and *alt_single_trans* is because the system does not respond in a symmetric way to a forcing increase or decrease due to the climate feedbacks and other physical processes such as changes in the oceanic and atmospheric circulation [*Hansen et al.*, 2005]. *alt_single_inst* is more similar to *G1_inst*, because both experiments that are subtracted describe the same TOA radiative imbalance. On the other hand in *G1_single_inst*, the combined experiments describe a very different TOA imbalance. The surface temperature responses in the single-forcing simulations are presented in Figures 4a–4f. Figures 4c–4f show that solar increase

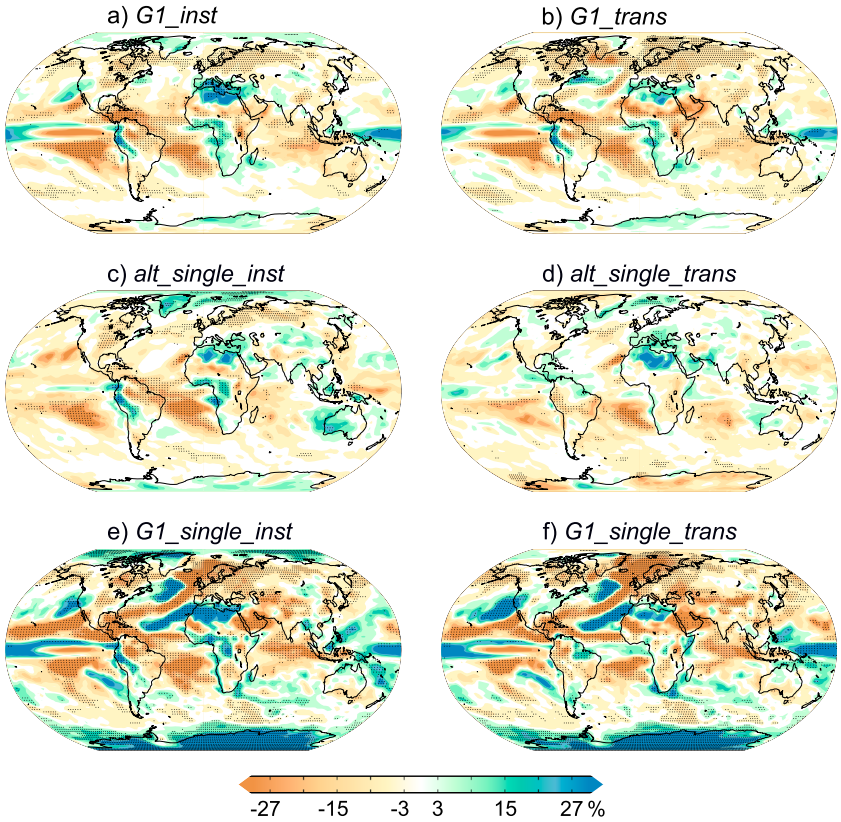

Figure 3. Maps of annual mean precipitation anomaly (%) averaged over the last 30 years of the respective geoengineering and combined geoengineering simulations: (a) *G1_inst*, (b) *G1_trans*, (c) *alt_single_inst*, (d) *alt_single_trans*, (e) *G1_single_inst*, and (f) *G1_single_trans*. Stippling indicates regions where the changes are significant at the 1% level. Significance level is estimated by using a Student's *t* test.

and decrease simulations are very different and that overall, solar increase simulations warm more in the Southern Hemisphere than the solar decrease simulations cool and vice versa in the Northern Hemisphere (see Figures 4g and 4h). This result is in agreement with *Hansen et al.* [2005], who performed simulations with solar irradiance increased and decreased by 2%. They suggest that the slower response of the oceans to a forcing decrease compared to a forcing increase might be a reason for the pattern shown in Figures 4g and 4h. They also further discuss that in a warming climate, the water vapor feedback is increasing while the sea ice-albedo feedback weakens with warming. *Manabe et al.* [1991] and *Stouffer* [2004] showed that overall the climate system responds faster to a cooling compared to a warming because a cooling promotes instabilities at the ocean surface and therefore triggers convection, while a warmer ocean surface is, in general, more stable since the penetration of heat into the ocean is inhibited. *Hargreaves et al.* [2007] showed that the sensitivity of the Model for Interdisciplinary Research on Climate (MIROC) AOGCM is larger to increasing compared to decreasing CO_2 concentrations, although in general, results from model runs with paleoclimate conditions can only be partly compared with the idealized simulations of solar forcing increase and decrease presented here. Other studies have shown that in simulations with Last Glacial Maximum conditions, an interhemispheric temperature contrast arises, with a cooling over the whole Northern Hemisphere and little response in the Southern Hemisphere [see, for example, *Ganopolski et al.*, 1998; *Chiang and Friedman*, 2012, and references therein]. *Broccoli et al.* [2006] showed that the atmospheric circulation reorganizes to some extent when one hemisphere becomes warmer or cooler than the other: the intertropical convergence zone (ITCZ) shifts toward the warmer hemisphere, which is accompanied by changes in the trade winds and an asymmetric response of the Hadley circulation. The ITCZ displacement is likely caused by changes in the way heat is exchanged between the midlatitudes and the tropics when one hemisphere becomes relatively warmer compared to the other [*Broccoli et al.*, 2006].

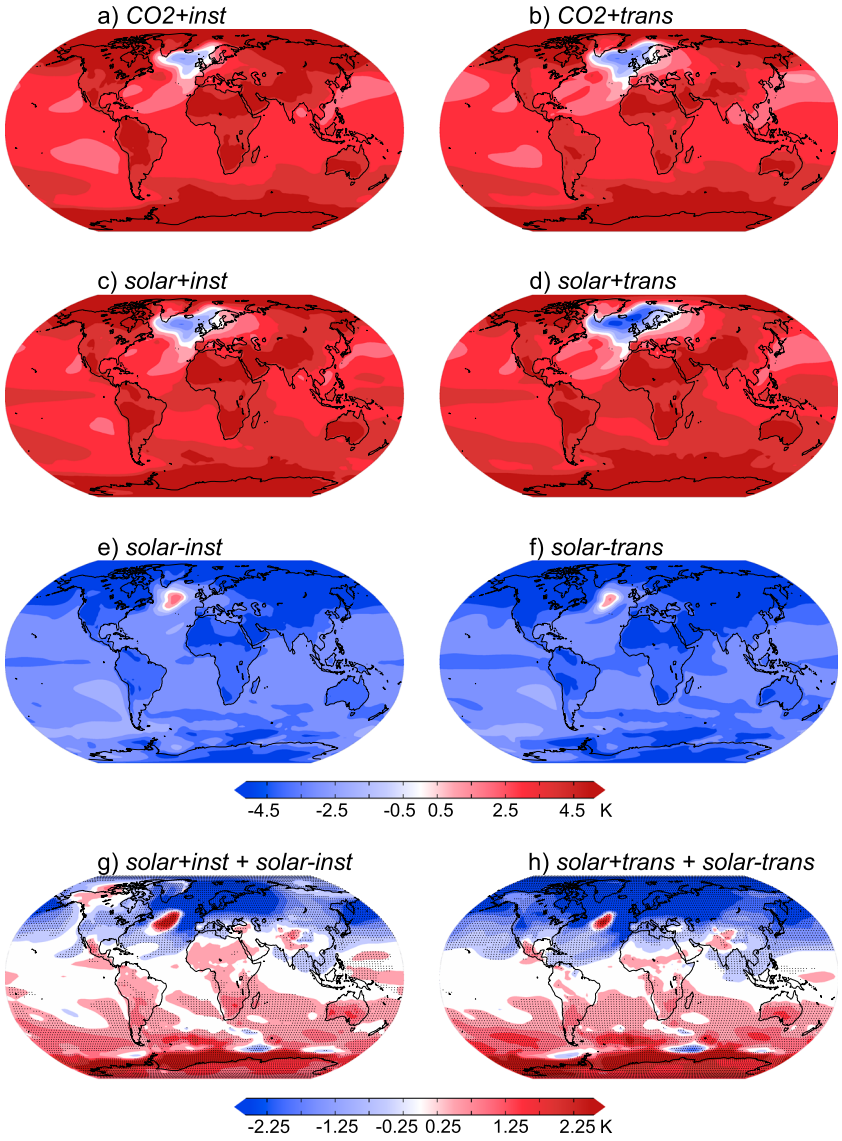

Figure 4. Maps of annual mean surface temperature anomaly (K): (a–f) in the single-forcing simulations and (g, h) as differences between solar increase and decrease simulation. The anomalies are averaged over the last 30 years of the instantaneous in Figures 4a, 4c, 4e, and 4g and the transient simulations in Figures 4b, 4d, 4f, and 4h. In Figures 4g and 4h, stippling indicates regions where the changes are significant at the 1% level. Significance level is estimated by using a Student's *t* test. The anomalies shown in Figures 4a–4f are all significant (except the white area), and therefore, no stippling has been added.

A detailed analysis of the physical mechanisms causing interhemispheric asymmetries is beyond the scope of this study, but we briefly discuss changes in poleward energy transport in forcing increase and decrease simulations here. In *solar-inst* and *solar-trans*, the surface temperature decrease is amplified in the polar regions, causing the pole-to-equator temperature gradient to become steeper while in *solar+inst*, *solar+trans*, *CO2+inst*, and *CO2+trans*, the pole-to-equator temperature gradient becomes flatter. Simply based on this fact, one would expect a stronger poleward energy transport in solar forcing decrease simulations and weaker poleward energy transport in solar forcing increase simulations. This is, however, not the case, as shown in Table 3; the poleward energy transport, calculated as the difference between the net energy flux anomaly at TOA and the net energy flux anomaly at surface for a Northern (50°N to 90°) and Southern (90°S to 50°S) Hemisphere box (similar to *Rugenstein et al.* [2013]), increases in *solar+inst* and *solar+trans* but decreases in *solar-inst* and *solar-trans*. The reason is that energy is not only transported as sensible heat but also as latent heat. In the solar forcing increase simulations, the atmosphere is warmer and

Table 3. Poleward Energy Transport in the Individual Geoengineering and Single-Forcing Simulations[a]

	Northward Energy Transport	Southward Energy Transport
G1_inst	−1.99	−1.8
G1_trans	−0.1	−1.71
CO2+inst	4.76	2.59
CO2+trans	6.49	2.1
solar+inst	8.58	4.54
solar+trans	9.61	4.15
solar-inst	−3.71	−4.78
solar-trans	−2.98	−4.66

[a]Units are in W/m^2; positive values indicate an energy transport from the equator to the poles, and negative values an energy transport from the poles to the equator.

holds more water vapor according to the Clausius-Clapeyron relation, resulting in an increase in the poleward energy transport, despite the fact that the large-scale atmospheric circulation (approximated by the pole-to-equator gradient) weakens. In the solar decrease simulations, the atmosphere is cooler and holds less water vapor, and even if the large-scale circulation is stronger, less energy can be transported northward. These results suggest that changes in water vapor are important in understanding the asymmetrical response of the system to a solar forcing increase or decrease.

In the Southern Hemisphere, *G1_single_inst* and *G1_single_trans* have a large positive anomaly in annual mean temperature over the Southern Ocean (see Figures 2e and 2f). This is partly due to the fact that the solar decrease simulations cool less than expected in the Southern Hemisphere, as described above [*Chiang and Friedman*, 2012]. Therefore, when the surface temperature anomaly patterns of *solar-inst* and *solar-trans* are added to those of *CO2+inst* and *CO2+trans*, the Southern Hemisphere appears warmer than in *G1_inst* and *G1_trans*. In addition, the response of the sea ice extent is also partly responsible for the strong positive anomalies in surface temperature around Antarctica, where sea ice is found in *G1_inst* and *G1_trans* (see Figures 2e and 2f). In the absence of sea ice, the ocean stores energy during summer months and releases it during winter months, while in the presence of sea ice, the atmosphere is isolated from the ocean and cannot receive energy from the ocean in winter [*Li et al.*, 2005]. Figures 2e and 2f show that the response of sea ice extent is not symmetric in the solar increase and decrease simulations. In *solar-inst* and *solar-trans*, the sea ice area continuously increases (even after the forcing remains constant in the transient case) and the sea ice-albedo feedback therefore continues to enhance the initial cooling throughout the simulations. In *solar+inst* and *solar+trans*, sea ice area decreases when the solar forcing increase is applied and the Southern Hemisphere rapidly becomes ice free. The sea ice area change is similar between simulations with CO_2 and solar forcing increases, and in both cases, the sea ice-albedo feedback, active in summer months, is partly suppressed once sea ice extent approaches zero (occurs at around year 30 in instantaneous and around year 80 in transient simulations; see Figures 2e and 2f). Consequently, in *alt_single_inst* and *alt_single_trans*, two similar climatic states in the Southern Ocean are combined, while in *G1_single_inst* and *G1_single_trans*, two different climatic states are added together. This is a reason why the temperature response looks similar between *alt_single_inst* and *alt_single_trans* and *G1_inst* and *G1_trans* (compare Figures 2a and 2b with Figures 2c and 2d).

Another major difference between the surface temperature pattern seen in *G1_single_inst* and *G1_single_trans*, as shown in Figure 2, is the strong cold anomaly in the North Atlantic. In surface warming simulations (i.e., *CO2+inst*, *CO2+trans*, *solar+inst*, and *solar+trans*), a cold anomaly of a few degrees is produced in the Labrador Sea and in the Greenland, Iceland, and Norwegian (GIN) Seas (see Figures 4a–4d). This temperature decrease is associated with the strong but gradual slowdown of the Atlantic Meridional Overturning Circulation (AMOC) in those scenarios (a decrease of around 17 sverdrup (10^6 m^3/s) (Sv)), as shown in Figures 5a and 5b. It should be noted that this relatively strong temperature decrease in the North Atlantic with global warming is a particular bias of CCSM3.5 and appears much weaker in CCSM4 [*Gent et al.*, 2011]. Similarly, the localized warming south of Greenland in *solar-inst* and *solar-trans* (see Figures 4e and 4f) is associated with the acceleration of the AMOC, which is at first relatively steep due to the promotion of convection [*Manabe et al.*, 1991; *Stouffer*, 2004]. However, as soon as a value of around 43 Sv is reached, the AMOC suddenly weakens and stabilizes at 37 Sv in *solar-inst* and 32 Sv *solar-trans*. No sudden anomaly changes are seen in North Atlantic sea surface salinity, density, or temperature that could explain this drop (not shown). However, Arctic sea ice area increases in solar decrease simulations (see Figures 5c and 5d). Studies showed that growing sea ice extent in the Arctic could prevent convection in the North Atlantic and hence cause a reduction of the AMOC strength [*Rose et al.*, 2013; *Li et al.*, 2005]. In a previous version of the model considered here, *Bitz et al.* [2007] identified that the recovery of the AMOC after a freshwater pulse in

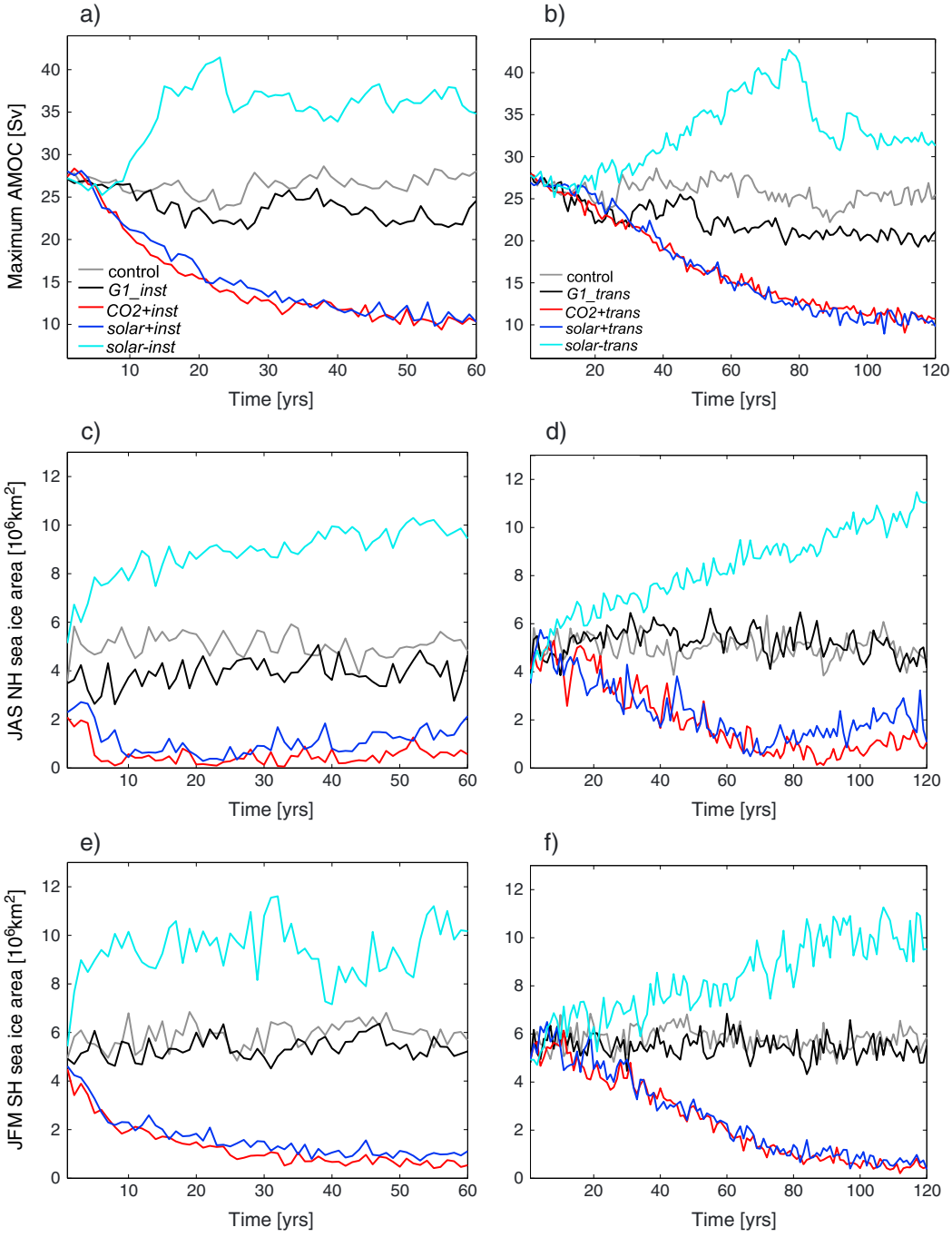

Figure 5. Time series of the anomalies compared to the control simulation of the maximum Atlantic meridional overturning circulation in (a) the instantaneous and (b) the transient simulations, the Northern Hemisphere sea ice area during June-August-September in (c) the instantaneous and (d) the transient simulations, and the Southern Hemisphere sea ice area during January-February-March in (e) the instantaneous and (f) the transient simulations.

the North Atlantic is slower in a colder climatic state compared to present due to the presence of sea ice over North Atlantic deep water formation regions. Areas of the GIN Seas start becoming sea ice covered in boreal winter months around year 10 and 70 in *solar-inst* and *solar-trans*, respectively, while the South Labrador sea becomes ice covered after the AMOC drop (not shown). The southward advance of Arctic sea ice in the GIN seas is therefore likely to be the reason for the sudden AMOC weakening but a model instability caused by the strong forcing applied cannot be entirely excluded.

Similarly, as in the Southern Hemisphere, the Arctic sea ice extent changes in the summer months (July-August-September); in forcing increase and decrease, simulations appear asymmetric as well. In *solar-inst* and *solar-trans*, sea ice extent increases throughout the course of the simulations, also after the forcing is kept constant (see Figures 5c and 5d). In *CO2+inst*, *CO2+trans*, *solar+inst*, and *solar+trans*, the Arctic becomes rapidly ice free in June-July-August, but during the last 30 years of the simulations, sea ice extent starts increasing again, in particular in the transient cases (see Figures 5c and 5d). This is due to the cold anomaly in the North Atlantic described above and is likely a cause of this model bias rather than a physical process that could be expected in the real world. Nevertheless, this implies that in *CO2+inst*, *CO2+trans*, *solar+inst*, and *solar+trans*, the sea ice-albedo feedback is either not active anymore when the Arctic is ice free (i.e., no further amplification of the initial warming) or, when sea ice extent starts increasing again, the sea ice-albedo feedback will be acting in the other direction (i.e., decreasing the warming in the Arctic). This leads to a relatively weak polar amplification toward positive temperature anomalies in *CO2+inst*, *CO2+trans*, *solar+inst*, and *solar+trans* compared to the polar amplification toward negative temperature anomalies in *solar-inst* and *solar-trans*, where the sea ice-albedo feedback is active and amplifying the initial cooling. It should be noted, however, that sea ice-albedo feedback is not the only feedback involved in polar amplification in both hemispheres and that water vapor and cloud feedbacks play an important role as well [*Graversen and Wang*, 2009]. Temperature anomalies in the northern high latitudes in *solar-inst* and *solar-trans* (Figures 4e and 4f) are more negative than the temperature anomalies in *CO2+inst*, *CO2+trans*, *solar+inst*, and *solar+trans* that are positive (Figures 4a–4d) for all the reasons described above. Adding the surface temperature anomaly pattern of *solar-inst* and *solar-trans* to *CO2+inst*, *CO2+trans* therefore leads to the overall too cold Northern Hemisphere in *G1_single_inst* and *G1_single_trans* compared to *G1_inst* and *G1_trans* as seen in Figures 2a and 2b and 2e and 2f.

3.2. Instantaneous Versus Transient

The global annual mean anomalies in the three instantaneous and the three transient cases presented in Table 2 are similar and of the same sign for *G1_inst* and *G1_trans*, but *alt_single_inst* and *G1_single_inst* have different anomaly signs for surface temperature and sensible heat compared to *alt_single_trans* and *G1_single_trans*. For the rest of this section, *G1_single_inst* and *G1_single_trans* will be left aside, since the previous section showed that they do not represent *G1_inst* and *G1_trans* as accurately as *alt_single_inst* and *alt_single_trans*.

The value of the solar constant decrease was chosen such that the global annual mean anomaly of temperature in *G1_inst* is close to zero. The same forcing changes were then applied to *G1_trans*, but the global annual mean temperature anomaly is negative (−0.24 K) at the end of the period considered. The simulation has not reached complete equilibrium yet as global annual mean net TOA energy flux is 0.19 W/m^2, which is a relatively large anomaly considering that throughout the 120 years of simulation, CO_2 and solar forcing should be well balanced as appears to be the case in *G1_inst*. It seems that the solar forcing decrease compensates well the CO_2 forcing increase if they are applied instantaneously, but when they are applied transiently, the effect of the solar forcing is amplified and overcompensates the warming caused by the CO_2 increase. It would be interesting to find out whether this behavior is seen in other models to investigate if this is a robust behavior. Nevertheless, given that the net TOA energy flux anomaly is positive in *G1_trans*, the system will warm until it approaches equilibrium and the global mean surface temperature anomaly will likely become zero.

Overall, the instantaneous and transient simulations have similar response patterns in terms of surface temperature and precipitation (see Figures 2 and 3a–3d). Figure 2 shows that the negative global annual mean anomaly in surface temperature in *G1_trans* described above arises from the cold North Atlantic and the western part of Eurasia. This is also seen at a smaller extent in *G1_inst* and is partly caused by the biased CCSM3.5 response to an AMOC weakening as described in the previous section, while in comparison, *alt_single_inst* and *alt_single_trans* have very well defined high latitudes warming and low latitudes cooling. The simulations combined to obtain *alt_single_inst* and *alt_single_trans* have comparable AMOC weakening, and therefore, the surface temperature anomalies in the North Atlantic to this weakening are similar. However, since polar amplification is slightly stronger in *CO2+inst* and *CO2+trans* compared to *solar+inst* and *solar+trans* due to the nature of the forcing agents, the cold bias in the North Atlantic appears slightly stronger in solar forcing increase simulations (see Figures 4a–4d). When the surface temperature pattern of *solar+inst* and *solar+trans* is subtracted from the pattern of *CO2+inst* and *CO2+trans*, the North Atlantic appears to have a positive temperature anomaly, as the rest of the northern high latitudes (see

Figures 2a–2d). This is different from what is seen in *G1_inst* and *G1_trans*, which have an AMOC weakening of around 5 Sv, causing a cooling in the North Atlantic (see Figures 2a and 2b). Previous studies have shown that a reduction in the AMOC results in a transiently increased ocean heat uptake, and as a consequence, a transient cooling in the atmosphere [*Knutti and Stocker*, 2000; *Raper et al.*, 2002]. The Northern Hemisphere in *G1_trans* appears significantly colder than in *G1_inst*, but as mentioned above, this difference will diminish as *G1_trans* reaches equilibrium.

4. Conclusions

The response to simple geoengineering simulations with a CO_2 forcing increase compensated by a solar constant decrease is investigated in this study. The two main goals are to identify potential differences between warming and cooling simulations and between the instantaneous and transient cases in order to assess how single-forcing simulations are best combined. The differences between CO_2 and solar forcing are also briefly discussed.

We show that in order to reproduce the climate response to the instantaneous and transient geoengineering simulations, it is more appropriate to subtract the response to a solar constant increase from the response to a CO_2 forcing increase than to add the response to a solar constant decrease to the response to a CO_2 forcing increase. Overall, the response to a solar constant increase or decrease is not regionally symmetric, as seen in paleoclimate studies [*Chiang and Friedman*, 2012]. The processes leading to the identified interhemispheric asymmetries are largely responsible for the fact that the response to an increase in solar constant, multiplied by −1, compensates better for an increase in CO_2 because those simulations have similar response patterns and similar magnitude of response. Although not investigated in this study, it is likely that the response to a CO_2 forcing increase or decrease is not symmetric as well [e.g., *Stouffer*, 2004]. A major reason for this outcome is that feedbacks are state dependent: for example, in the extreme case, the sea ice-albedo feedback is no longer relevant if the whole ocean surface is ice covered or ice free year round. Further, sea ice-albedo feedbacks take place in different regions in the solar forcing increase and decrease simulations: in a warming scenario, the response will be large where there was sea ice before, and in a cooling case it will be large where there was no sea ice to begin with. Changes in the oceanic circulation in the Atlantic are also shown to behave asymmetrically: there is a lower bound when the AMOC is shut down (deep water formation cannot be negative), but there is also probably a physical upper bound, as waters will not be able to accelerate indefinitely. In the model used, the upper bound appears to be around 43–44 Sv. However, the AMOC did not stabilize at this upper bound but to a somewhat lower value, probably due to the southward extent of the Arctic sea ice. Overall, it is likely that the oceanic circulation, in general, does not behave symmetrically to forcing increases or decreases, which would lead to an additional atmospheric response caused by oceanic circulation and not by the forcing change directly. With different spatial response patterns to a solar forcing increase or decrease, the local temperature gradients also change and thus, most likely the atmospheric circulation patterns.

As expected, combined response patterns do not replicate exactly all the local anomalies of geoengineering simulations. One reason is that in the geoengineered simulations, global annual mean surface temperature remains relatively constant, implying that feedbacks are partly suppressed compared to the forcing increase and decrease simulations. In addition, the combined geoengineering simulations are missing the interaction between the two forcing agents. In particular, our results suggest that the response to solar forcing is stronger when solar forcing is combined with CO_2 forcing, in agreement with *Meehl et al.* [2003]. This nonlinearity in response to individual forcing, along with the asymmetry of the climate response to forcing increase and decrease presented in this study is of importance for research fields where assumptions are made about the linearity of the response, like pattern scaling and attribution studies.

Finally, the global mean measures of instantaneous and transient simulations are found to be very similar at the end of the simulations when the climate system is in quasi-equilibrium.

We use simulation setups similar to the ones used in GeoMIP [*Kravitz et al.*, 2011], but the forcings applied here still are strong forcings to the climate system, and it is possible that the responses would appear more symmetrical to weaker forcings like a doubling of CO_2. The exact values and patterns presented in this study are probably model dependent (in particular the cold anomalies in the North Atlantic in forcing increase simulations), and a project similar as GeoMIP to intercompare models on scenarios designed to test the linearities in response to forcings is much needed. These results also provide further evidence that the

feedbacks are state dependent [*Senior and Mitchell*, 2000] and regionally dependent [*Boer and Yu*, 2003a, 2003b; *Boer et al.*, 2007]. This has central implications for interpreting the potential regional gains and losses in terms of climatic conditions or food production, for example, in studies about geoengineered futures. The response of the climate system is complex as shown in this study, which prevents arguing in terms of global budgets, where losses can be leveraged by gains. Because the forcing agents interact with each other, because the responses of the climate system are not symmetric and do not add linearly and because the feedbacks are state dependent, it cannot be assumed that in the real world the regional CO_2-induced climate change could simply be compensated by a decrease in incoming shortwave radiation, as assumed globally for example by *Wigley* [2006].

Acknowledgments
The National Center for Atmospheric Research Community Climate System Model is openly available at https://www2.cesm.ucar.edu/models/scientifcally-supported. For data requests, please contact Nathalie Schaller (nathalie.schaller@ouce.ox.ac.uk).

References

Andrews, T., P. M. Forster, O. Boucher, N. Bellouin, and A. Jones (2010), Precipitation, radiative forcing and global temperature change, *Geophys. Res. Lett.*, *37*, L14701, doi:10.1029/2010GL043991.

Bala, G., P. B. Duffy, and K. E. Taylor (2008), Impact of geoengineering schemes on the global hydrological cycle, *Proc. Natl. Acad. Sci. U.S.A.*, *105*(22), 7664–7669, doi:10.1073/pnas.0711648105.

Bala, G., K. Caldeira, and R. Nemani (2010), Fast versus slow response in climate change: Implications for the global hydrological cycle, *Clim. Dyn.*, *35*(2-3), 423–434, doi:10.1007/s00382-009-0583-y.

Ban-Weiss, G. A., and K. Caldeira (2010), Geoengineering as an optimization problem, *Environ. Res. Lett.*, *5*(3), 034,009, doi:10.1088/1748-9326/5/3/034009.

Barnett, T., et al. (2005), Detecting and attributing external influences on the climate system: A review of recent advances, *J. Clim.*, *18*(9), 1291–1314.

Bitz, C. M., J. C. H. Chiang, W. Cheng, and J. J. Barsugli (2007), Rates of thermohaline recovery from freshwater pulses in modern, Last Glacial Maximum, and greenhouse warming climates, *Geophys. Res. Lett.*, *34*, L07708, doi:10.1029/2006GL029237.

Boer, G. J., and B. Yu (2003a), Dynamical aspects of climate sensitivity, *Geophys. Res. Lett.*, *30*(3), 1135, doi:10.1029/2002GL016549.

Boer, G. J., and B. Yu (2003b), Climate sensitivity and climate state, *Clim. Dyn.*, *21*(2), 167–176, doi:10.1007/s00382-003-0323-7.

Boer, G. J., M. Stowasser, and K. Hamilton (2007), Inferring climate sensitivity from volcanic events, *Clim. Dyn.*, *28*(5), 481–502, doi:10.1007/s00382-006-0193-x.

Broccoli, A. J., K. A. Dahl, and R. J. Stouffer (2006), Response of the ITCZ to Northern Hemisphere cooling, *Geophys. Res. Lett.*, *33*, L01702, doi:10.1029/2005GL024546.

Cao, L., G. Bala, and K. Caldeira (2012), Climate response to changes in atmospheric carbon dioxide and solar irradiance on the time scale of days to weeks, *Environ. Res. Lett.*, *7*(3), 34,015–34,015.

Chadwick, R., and P. Good (2013), Understanding nonlinear tropical precipitation responses to CO_2 forcing, *Geophys. Res. Lett.*, *40*, 4911–4915, doi:10.1002/grl.50932.

Chiang, J. C. H., and A. R. Friedman (2012), Extratropical cooling, interhemispheric thermal gradients, and tropical climate change, *Ann. Rev. Earth Planet. Sci.*, *40*, 383–412, doi:10.1146/annurev-earth-042711-105545.

Collins, W. D., et al. (2006), The Community Climate System Model version 3 (CCSM3), *J. Clim.*, *19*, 2122–2143.

Crutzen, P. J. (2006), Albedo enhancement by stratospheric sulfur injections: A contribution to resolve a policy dilemma?, *Clim. Change*, *77*(3-4), 211–219, doi:10.1007/s10584-006-9101-y.

Fischer, E. M., D. M. Lawrence, and B. M. Sanderson (2011), Quantifying uncertainties in projections of extremes—A perturbed land surface parameter experiment, *Clim. Dyn.*, *37*(7-8), 1381–1398, doi:10.1007/s00382-010-0915-y.

Fyfe, J. C., J. N. S. Cole, V. K. Arora, and J. F. Scinocca (2013), Biogeochemical carbon coupling influences global precipitation in geoengineering experiments, *Geophys. Res. Lett.*, *40*, 651–655, doi:10.1002/grl.50166.

Ganopolski, A., S. Rahmstorf, V. Petoukhov, and M. Claussen (1998), Simulation of modern and glacial climates with a coupled global model of intermediate complexity, *Nature*, *391*(6665), 351–356.

Gent, P. R., S. G. Yeager, R. B. Neale, S. Levis, and D. A. Bailey (2010), Improvements in a half degree atmosphere/land version of the CCSM, *Clim. Dyn.*, *34*(6), 819–833, doi:10.1007/s00382-009-0614-8.

Gent, P. R., et al. (2011), The Community Climate System Model version 4, *J. Clim.*, *24*(19), 4973–4991, doi:10.1175/2011JCLI4083.1.

Good, P., J. M. Gregory, and J. A. Lowe (2011), A step-response simple climate model to reconstruct and interpret AOGCM projections, *Geophys. Res. Lett.*, *38*, L01703, doi:10.1029/2010GL045208.

Govindasamy, B., and K. Caldeira (2000), Geoengineering Earth's radiation balance to mitigate CO_2-induced climate change, *Geophys. Res. Lett.*, *27*(14), 2141–2144, doi:10.1029/1999GL006086.

Graversen, R. G., and M. Wang (2009), Polar amplification in a coupled climate model with locked albedo, *Clim. Dyn.*, *33*(5), 629–643, doi:10.1007/s00382-009-0535-6.

Hansen, J., et al. (2005), Efficacy of climate forcings, *J. Geophys. Res.*, *110*, D18104, doi:10.1029/2005JD005776.

Hargreaves, J. C., A. Abe-Ouchi, and J. D. Annan (2007), Linking glacial and future climates through an ensemble of GCM simulations, *Clim. Past*, *3*(1), 77–87.

Jonko, A. K., K. M. Shell, B. M. Sanderson, and G. Danabasoglu (2012), Climate feedbacks in CCSM3 under changing CO_2 forcing. Part I: Adapting the linear radiative kernel technique to feedback calculations for a broad range of forcings, *J. Clim.*, *25*(15), 5260–5272, doi:10.1175/JCLI-D-11-00524.1.

Knutti, R., and T. F. Stocker (2000), Influence of the thermohaline circulation on projected sea level rise, *J. Clim.*, *13*(12), 1997–2001, doi:10.1175/1520-0442(2000)013<1997:IOTTCO>2.0.CO;2.

Kravitz, B., A. Robock, O. Boucher, H. Schmidt, K. E. Taylor, G. Stenchikov, and M. Schulz (2011), The Geoengineering Model Intercomparison Project (GeoMIP), *Atmos. Sci. Lett.*, *12*(2), 162–167, doi:10.1002/asl.316.

Kravitz, B., et al. (2013a), Climate model response from the Geoengineering Model Intercomparison Project (GeoMIP), *J. Geophys. Res. Atmos.*, *118*, 8320–8332, doi:10.1002/jgrd.50646.

Kravitz, B., et al. (2013b), An energetic perspective on hydrological cycle changes in the Geoengineering Model Intercomparison Project, *J. Geophys. Res. Atmos.*, *118*, 13,087–13,102, doi:10.1002/2013JD020502.

Lawrence, D. M., P. E. Thornton, K. W. Oleson, and G. B. Bonan (2007), The partitioning of evapotranspiration into transpiration, soil evaporation, and canopy evaporation in a GCM: Impacts on land-atmosphere interaction, *J. Hydrometeorol.*, *8*(4), 862–880, doi:10.1175/JHM596.1.

Li, C., D. S. Battisti, D. P. Schrag, and E. Tziperman (2005), Abrupt climate shifts in Greenland due to displacements of the sea ice edge, *Geophys. Res. Lett.*, *32*, L19702, doi:10.1029/2005GL023492.

MacMartin, D. G., D. W. Keith, B. Kravitz, and K. Caldeira (2013), Management of trade-offs in geoengineering through optimal choice of non-uniform radiative forcing, *Nat. Clim. Change*, *3*(4), 365–368, doi:10.1038/NCLIMATE1722.

Manabe, S., R. J. Stouffer, M. J. Spelman, and K. Bryan (1991), Transient responses of a coupled ocean atmosphere model to gradual changes of atmospheric CO_2: 1. Annual mean response, *J. Clim.*, *4*(8), 785–818, doi:10.1175/1520-0442(1991)004<0785:TROACO>2.0.CO;2.

McCusker, K. E., D. S. Battisti, and C. M. Bitz (2012), The climate response to stratospheric sulfate injections and implications for addressing climate emergencies, *J. Clim.*, *25*(9), 3096–3116, doi:10.1175/JCLI-D-11-00183.1.

Meehl, G. A., W. M. Washington, T. M. L. Wigley, J. M. Arblaster, and A. Dai (2003), Solar and greenhouse gas forcing and climate response in the twentieth century, *J. Clim.*, *16*(3), 426–444.

Meehl, G. A., W. M. Washington, C. M. Ammann, J. M. Arblaster, T. M. L. Wigley, and C. Tebaldi (2004), Combinations of natural and anthropogenic forcings in twentieth-century climate, *J. Clim.*, *17*(19), 3721–3727.

Mitchell, T. D. (2003), Pattern scaling—An examination of the accuracy of the technique for describing future climates, *Clim. Change*, *60*(3), 217–242.

Raper, S. C. B., J. M. Gregory, and R. J. Stouffer (2002), The role of climate sensitivity and ocean heat uptake on AOGCM transient temperature response, *J. Clim.*, *15*(1), 124–130, doi:10.1175/1520-0442(2002)015<0124:TROCSA>2.0.CO;2.

Ricke, K. L., G. Morgan, and M. R. Allen (2010), Regional climate response to solar-radiation management, *Nat. Geosci.*, *3*(8), 537–541, doi:10.1038/ngeo915.

Rose, B. E. J., D. Ferreira, and J. Marshall (2013), The role of oceans and sea ice in abrupt transitions between multiple climate states, *J. Clim.*, *26*, 2862–2879, doi:10.1175/JCLI-D-12-00175.1.

Rugenstein, M. A. A., M. Winton, R. J. Stouffer, S. M. Griffies, and R. Hallberg (2013), Northern high latitude heat budget decomposition and transient warming, *J. Clim.*, *26*(2), 609–621, doi:10.1175/JCLI-D-11-00695.1.

Schaller, N., J. Cermak, M. Wild, and R. Knutti (2013), The sensitivity of the modeled energy and water cycles to CO_2 and solar forcing, *Earth Syst. Dyn.*, *4*, 253–266, doi:10.5194/esd-4-253-2013.

Schmidt, H., et al. (2012), Solar irradiance reduction to counteract radiative forcing from a quadrupling of CO_2: Climate responses simulated by four Earth System Models, *Earth Syst. Dyn.*, *3*, 63–78.

Schneider, S. H. (1996), Geoengineering: Could or should we do it?, *Clim. Change*, *33*(3), 291–302, doi:10.1007/BF00142577.

Sedlacek, J., R. Knutti, O. Martius, and U. Beyerle (2012), Impact of a reduced Arctic sea ice cover on ocean and atmospheric properties, *J. Clim.*, *25*(1), 307–319, doi:10.1175/2011JCLI3904.1.

Senior, C. A., and J. F. B. Mitchell (2000), The time-dependence of climate sensitivity, *Geophys. Res. Lett.*, *27*(17), 2685–2688, doi:10.1029/2000GL011373.

Stott, P. A., S. F. B. Tett, G. S. Jones, M. R. Allen, J. F. B. Mitchell, and G. J. Jenkins (2000), External control of 20th century temperature by natural and anthropogenic forcings, *Science*, *290*(5499), 2133–2137, doi:10.1126/science.290.5499.2133.

Stott, P. A., J. F. B. Mitchell, M. R. Allen, T. L. Delworth, J. M. Gregory, G. A. Meehl, and B. D. Santer (2006), Observational constraints on past attributable warming and predictions of future global warming, *J. Clim.*, *19*(13), 3055–3069.

Stouffer, R. J. (2004), Time scales of climate response, *J. Clim.*, *17*(1), 209–217, doi:10.1175/1520-0442(2004)017<0209:TSOCR>2.0.CO;2.

Tilmes, S., et al. (2013), The hydrological impact of geoengineering in the Geoengineering Model Intercomparison Project (GeoMIP), *J. Geophys. Res. Atmos.*, *118*, 11,036–11,058, doi:10.1002/jgrd.50868.

Vaughan, N. E., and T. M. Lenton (2011), A review of climate geoengineering proposals, *Clim. Change*, *109*(3-4), 745–790, doi:10.1007/s10584-011-0027-7.

Wigley, T. M. L. (2006), A combined mitigation/geoengineering approach to climate stabilization, *Science*, *314*(5798), 452–454, doi:10.1126/science.1131728.